Helmholtz-Zentrum Geesthacht
Zentrum für Material- und Küstenforschung

Final Draft
of the original manuscript:

Schaper, J.G.; Wolff, M.; Wiese, B.; Ebel, T.; Willumeit-Römer, R.:
Powder metal injection moulding and heat treatment of AZ81 Mg alloy.
In: Journal of Materials Processing Technology. Vol. 267 (2019) 241 - 246.
(DOI: /10.1016/j.jmatprotec.2018.12.015)
First published online by Elsevier: 12.12.2018

https://dx.doi.org/10.1016/j.jmatprotec.2018.12.015

Powder Metal Injection Moulding and Heat Treatment of AZ81 Mg Alloy

By *Johannes G. Schaper* [a, b, c], *Martin Wolff* [b], *Björn Wiese* [b], *Thomas Ebel* [b], *Regine Willumeit-Römer* [b]

(a) corresponding author: *Johannes G. Schaper, E-mail: Johannes.Schaper@element22.de*
(b) *Helmholtz-Zentrum Geesthacht Centre for Materials and Coastal Research GmbH Max-Planck Str. 1, 21502, Geesthacht, Germany*
(c) *Element 22 GmbH, Wischhofstr. 1-3, 24148, Kiel*

Ongoing research has proven that Mg alloys can be introduced into the metal injection moulding process for production of small parts in high quantities and of complex shape for medical as well as lightweight applications. Previous development studies have been conducted using Mg and Mg-Ca alloys intended for medical application. However, progress towards implementation of the process for technical and lightweight applications alloys with higher strength are needed. Therefore, in this study processing of conventional AZ81 alloy by MIM was successfully developed. Using this alloy, a yield strength of approximately 120 MPa and an ultimate tensile strength of approximately 255 MPa with elongation at fracture of approximately 7% was achieved. T4 heat treatment at 420 °C for 10 hours does not reveal a positive influence on the mechanical properties due to grain growth effect. This is in contrast to conventional material like for example as cast, where T4 heat treatment is known to improve the mechanical properties especially elongation at fracture.

Keywords: Magnesium, Sintering, Mechanical Properties, Grain Growth, Liquid Phase

Declarations of interest: none.

Introduction

Kainer (2003) summed up that magnesium alloys have a great potential to be used as metallic lightweight materials in a broad variety of applications such as automotive, aviation, consumer and aerospace as well as degradable implant material for biomedical applications. Mordike and Ebert (2001) explained that Mg is the lightest structural metal and therefore of high interest for lightweight construction in all fields of technical applications. Witte et al. (2008) recognized that its good biocompatibility in combination with its degradation products which are essential in the human body makes Mg attractive as degradable metallic material for implant applications. In this framework, metal injection moulding (MIM) implicates a high potential for an economic production of small, complex near net shape parts in high quantities. MIM possess the possibility to produce parts with different porosities, from open porous up to total dense, in net shape or near net shape quality in high volumes with nearly no material loss due to post treatment as stated by German (1990). To combine the benefits of the magnesium alloys with the ones of the MIM technology MIM of Mg has been developed recently by Wolff et al. (2018).

According to German (1990) the MIM process can be divided into five process steps. The first step is to produce a so called feedstock which is typically a mixture of the metal powder and organic binder components. This feedstock is then processed using an injection moulding machine to produce a so called green part. This green part typically already contains all the geometrical features of the part to be produced with a scale factor based on the estimated shrinkage due to the consolidation of the powder. The green part is then typically treated in a solvent to remove the major part of the binder. After extraction of the major binder components the so called brown part consist of the metal powder and the so called backbone polymer. The polymer is removed by thermal treatment prior to the final sintering step.

Using magnesium in the MIM process thermal debinding (Wolff et al. 2016a) and sintering

(Wolff et al. 2016b) are the most critical steps due to its high reactivity and affinity of magnesium to oxygen.

Wolff et al. (2010) as well as Burke at al. (2013) found out that due to its stable oxide layer, acting as a diffusion barrier, sintering of Mg and its alloys is sophisticated and needs to be conducted under high purity oxygen free atmospheres for elevated times with temperatures close to the melting point. The use of high vacuum atmospheres as used for MIM of Ti as reported by Obasi et al. (2010) cannot be used for Mg due to its high vapour pressure, which would lead to evaporation of samples at higher temperatures (Ha and Kim, 2006). To maintain high purity atmospheres during sintering high purity argon in combination with a labyrinth-like crucible set up with Mg getter material is used when sintering Mg (Wolff et al. 2010). Ca can be used as an alloying element to produce a liquid phase during sintering to accelerate the densification of the material (Wolff et al. 2010). Numerous publications have focused on the production of porous Mg compounds by sintering aiming mostly for medical applications. Wen et al. (2001) and Wen et al. (2004) achieved an open porous structure with porosities between 35% and 55% using a space holder technique. Pore size was varied between 70-400 µm. The peak stress in compression tests are reported to be in the range of 17 MPa. However, the strength of the unsintered (green parts) was not reported. Furthermore, according to the experience of Wolff et al. (2010) and Schaper et al. (2017), the short sintering time of 2 hours and a low sintering temperature of around 500 °C is not sufficient for successful sintering of pure Mg. Čapek and Vojtěch, (2013) and Čapek and Vojtěch, (2014) also produced samples using a space holder technique. Sintering was carried out at a temperature of 550 °C for 3, 6, 12 and 24 hours in technical Ar as well as in atmosphere gettered by Mg powder resulting in porosities between 24 vol.% and 29 vol.%. It is reported that the purity of the sintering atmosphere has a major influence on the sintering results. The maximum ultimate compressive strength was measured to be 69 MPa after sintering for 24 hours under gettered Ar atmosphere. Green part samples showed a strength of 20 MPa. However, it is hard to compare these results of Čapek and Vojtěch

(2013, 2014) and Wen et al. (2001, 2004) as the force used for compacting the samples before sintering was different between the works of these two groups.

Other studies focus on achieving a low residual porosity by conventional sintering techniques. Burke et al. (2013) compacted spherical Mg powder with a rather high compaction pressure of 500 MPa before sintering. Densities after sintering for 40 and 360 min at 600 °C were around 95% of the theoretical density. Maximum ultimate tensile strength was reported to be 72 MPa. Nishiyama et al. (2003) investigated the damping properties of a Mg alloy containing Cu and Mn. Samples were pressed at a pressure of 300 MPa and sintered at 475-645 °C in Ar. The sintering time was not reported. Residual porosity was reported to be approximately 1% after liquid phase sintering at 625 °C. Maximum bending strength was reported to be 291 MPa. Wolff et al. (2010) could achieve sintering porosities around 2% with compression yield strength of 69 MPa and ultimate compression strength of 255 MPa when sintering Mg-1Ca for 64 hours at 610 °C.

Once sintering of Mg was proven feasible the material could be introduced into the MIM process. Initial experiments were performed by Wolff et al. (2011) using a polyethylene-wax bases binder system, which resulted in poor sintering performance of the material compared to binder free samples. A sintering inhibiting effect could be traced back to the used polyethylene. Polypropylene-wax based binder systems do not show such negative influences on the sintering performance of the Mg powder particles (Wolff et al. 2016b). Optimization of all process steps of the MIM route in particular the heat treatment steps like thermal debinding and sintering led to good sintering results as reported by Wolff et al. (2016b) and Schaper et al. (2017). Using a Mg-0.9Ca alloy in combination with a polypropylene based binder system, residual porosities around 3% leading to mechanical satisfying mechanical properties (yield strength: 65 MPa, ultimate tensile strength: 160 MPa, elongation at fracture 7%) could be achieved (Wolff et al. 2016b).

Harun et al. (2010) investigated the rheological properties and solvent debinding (Harun at al. 2012) of Mg feedstocks with polyethylene and palm stearin based binder systems but did not publish any results about the most critical process steps like thermal debinding and sintering. It is probable that the polyethylene based binder approach did not lead to sufficient sintering results due to the negative influence of polyethylene on the sintering of Mg as reported by Wolff et al. (2011).

Mg-Ca alloys investigated up to date need long sintering times of up to 64 hours to achieve a porosity below 5% and offer only a moderate ultimate tensile strength of around 140 MPa (Schaper et al. 2017). Both factors make MIM of Mg-Ca alloys unattractive for technical applications. To overcome these drawbacks in this study MIM processing of AZ81 as an example of more complex alloys with higher strength and improved sintering kinetics is investigated.

Experimental Methods

Spherical AZ81 powder was received from SFM SA (Martigny, Switzerland) with a composition of 7.7 wt.% Al, 0.6 wt.% Zn, 0.3 wt.% Mn, Mg bal. (according to the manufacturer's analysis). Feedstock was prepared with a powder loading of 64 vol.% using a polypropylene wax based binder system (35 wt.% polypropylene (Total, Belgium), 60 wt%. paraffin wax (Sigma-Aldrich, Germany), 5 wt.% stearic acid (Sigma-Aldrich, Germany)). Feedstock preparation was performed under a protective Ar atmosphere using a glove box system (MBraun, Unilab, Germany), a heating plate and a planetary mixer (Thinky ARE-250, Japan). Feedstock production was followed by homogenizing the feedstock by extrusion through the plasticizer unit of the injection moulding machine (Arburg Allrounder 320S, Germany) followed by granulation using a cutting mill (Wanner B08.10f, Germany). Dog bone shape tensile test specimens according to ISO 2740-B were produced using the injection moulding machine. The resulting green parts were solvent debound using hexane at 40 °C for

15 hours (Lömi EBA50, Germany) to remove the wax. The resulting brown parts were placed in a labyrinth-like crucible set up as described by Schaper at al. (2017) with getter material (Mg grit particle size 0.06-0.3 mm purity >98.5%, Merck, Germany). Thermal debinding and sintering took place in a hot wall retort furnace (MUT RRO350-900, Germany). Thermal debinding was performed by increasing the temperature from 350 °C to 460 °C with a heating rate of 0.5 K min^{-1} with an alternating pressure between 5 and 30 mbar at a Ar+5 vol.% H_2 purge gas flow of 0.5 l min^{-1} followed by vacuum up to 500 °C. At 500 °C pure argon (Ar6.0) up to a pressure of 30 mbar was introduced while the temperature rose to the sintering temperature of 605 °C with a heating rate of 2 K min^{-1}. The sintering temperature was maintained for 4 hours followed by furnace cooling (approx. 5 K/min 600-300 °C, 3 °K/min 300-200 °C, 1 K/min 200-100 °C) under Ar at ambient pressure. **Figure 1** shows the produced dog bone shape tensile test specimens after injection moulding (green part) and after sintering. The shrinkage due to the densification during sintering is clearly visible and the sintered part shows a shiny metal surface.

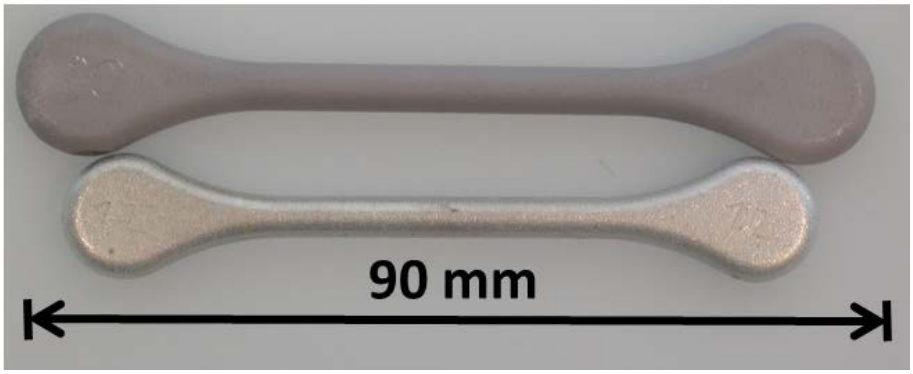

Figure 1. Dog bone shape tensile test specimen according to ISO 2740-B: green part (top) and sintered part (bottom). Material: AZ81.

Shrinkage *S* was determined by comparing the length of the green and sintered parts by using a calliper (Mahr 16EX, Germany) according to **equation 1** were L_g is the length of the green part and L_s the length of the sintered part. The residual porosity was determined using image analysing software by analysing the phase fraction with adjustable threshold for the greyscale

(analySIS pro, Olympus Soft Imaging Solutions, Germany) averaged from five scanning electron microscopy (SEM) micrographs with a view field of 1380 x 1200 µm of 200x.

$$S = (L_g - L_s) / L_g \quad (1)$$

T4 heat treatments were performed on one set of samples (n=6) using a retort furnace (Xerion XRetort, Germany) at 420 °C for 10 hours under argon followed by water quenching (after suggestion of Avedesian and Baker, 1999, T4 heat treatment of AZ81 and the calculated phase diagram).

Tensile tests took place using a universal testing machine (Schenck Trebel RM100, Germany) according to DIN EN ISO 6892-1:2009 B with a traverse speed of 0.2 mm min^{-1}. Microstructural analyses were performed on non-tested samples after grinding and polishing using (SEM) equipped with energy dispersive X-ray spectroscopy (EDXS) (Tescan Vega3, operating at 15 kV in the secondary electrons (SE) mode) as well as electron backscatter diffraction (EBSD) measurements (Carl Zeiss AG, Typ Ultra 55 SEM equipped with EBSD).

Results and Discussion

After sintering the samples show a silver shiny metal surface as shown in **Figure 1**. Sintering of the AZ81 samples results in a longitudinal shrinkage of 13.8% ±0.1% with a residual porosity of 1.3%. This porosity is low compared to the porosity of previously sintered Mg-0.9Ca MIM samples, which obtain a residual porosity of around 3% after sintering for 64 hours at 637 °C (Wolff et al. 2016b). The fact that sintering the AZ81 alloy for only 4 hours at 605 °C results in low porosity shows the high sintering activity of this alloy. The reason for the high sintering activity is presumably the higher liquid phase amount during sintering compared to Mg-0.9Ca. Thermodynamic calculations were performed at the sintering temperature of AZ81 and Mg-0.9Ca, to compare the difference in the liquid phase fraction. All calculations were done using the Pandat™ 2017 software package with PanMagnesium 2017 database (CompuTherm, 2017). A point calculation was conducted for AZ81 (7.7 wt.% Al, 0.6 wt.% Zn, 0.3 wt.% Mn, Mg bal.)

at 605 °C and Mg-0.9Ca (0.9 wt.% Ca, Mg bal.) at 637 °C (Schaper et al. 2017). The liquid phase fraction in AZ81 is 89.5 wt% and in Mg-0.9Ca is 37.3 wt% at sintering temperature. The higher amount of liquid phase increased the sintering activity due to the wetting of the powder and faster diffusion compared to diffusion in solid. If the amount of liquid phase is increased more powder is surrounded by this liquid phase, which increases the diffusion process by more contact between the powders. This leads to a sintering process without necking in the first stage of sintering. It is hypothesised that the wetting angle of AZ81 liquid phase is lower compared to that of Mg-0.9Ca, resulting in higher acceptable liquid phase amount without exuding liquid phase from the part. However, to prove this hypothesis more investigations like contact angle measurements, are needed. Sintering for a longer time at a temperature of 605 °C even leads to shape loss, as previously reported by Schaper et al. (2017). This can be explained due to the high liquid phase amount during sintering in combination with shrinkage. During shrinking the porosity of the compound decreases. When the ratio of liquid phase and porosity exceeds a certain value shape loss starts.

Figure 2 shows the microstructure of the MIM samples using the SEM. Residual porosity with different pore size can be clearly identified (black arrows). The former powder particle boundaries are still visible (see black marking). The EDXS results of the measurements on **Figure 2(b)** are shown in **Table 1**. The bright phases (see cross 1 in Fig. 2(b)) show a high content of Al and Mn. The atomic composition equals to a Al:Mn ratio of 61:31 which is close to the phase Al_8Mn_5. This is a stable phase formed at higher temperatures in the Mg-Al-Zn-Mn system as reported by Ohno et al. (2006). The smaller bright phases at the former particle boundaries (see cross 2) reveal high amounts of oxygen. Thus, they can be assumed to be Mg-oxides. The former particle boundaries (see cross 4) show higher Al and O concentrations compared to the matrix (see cross 3). The increased oxygen content can be explained by the fact that the stable Mg-oxides of the former powder surfaces stay in place during the sintering process. The stability of oxide layers on Mg powder was also reported in the work of Wiese et

al. (2014) above the melting temperature (at 700 °C for 5 min) of the Mg-Al-Ca-O system. The increased Al content is presumably caused by the formation of $Mg_{17}Al_{12}$ phase at the former particle boundaries (Avedesian and Baker, 1999).

Figure 3 shows the microstructure of a MIM+T4 sample with EDXS point measurements. The corresponding EDXS results for **Figure 3** are given in **Table 2.** The MIM+T4 heat treated samples show comparable results in the EDXS measurements with a slightly higher Al content inside the particles (see cross 3 in **Figure 3**) probably caused by the higher solubility of Al in Mg at the heat treatment temperature followed by rapid cooling (Ohno et al. 2006). The Al-Mn rich phases appear to be slightly bigger compared to the as-MIM condition with a comparable composition. At the former particle boundaries oxides and increased Al content are apparent as demonstrated for the MIM material.

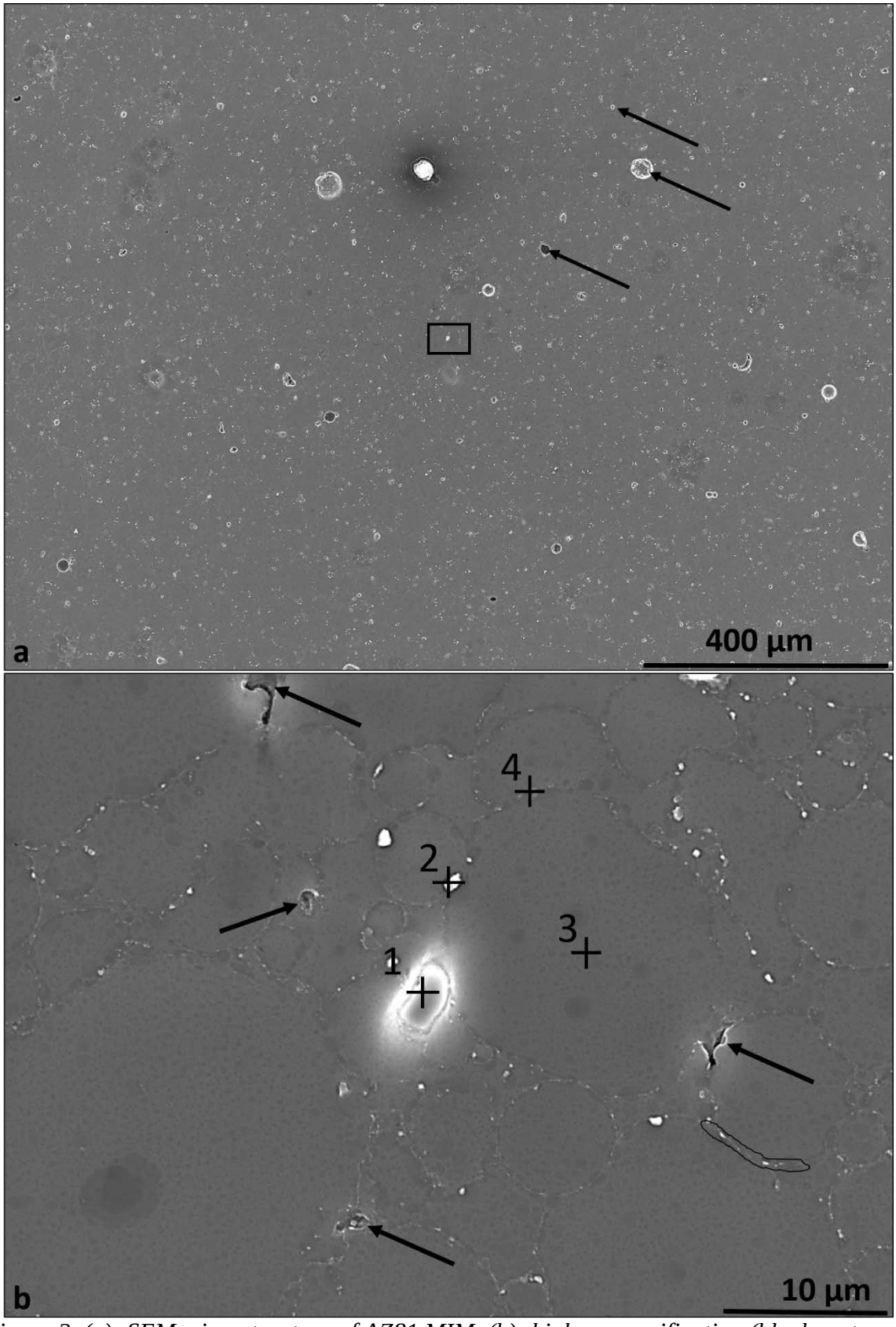

Figure 2. (a): SEM microstructure of AZ81 MIM, (b): higher magnification (black rectangle from (a)) in SE mode.

Table 1. Results of EDXS measurements on Figure 2

Point	Mg [wt.%]	Al [wt.%]	Zn [wt.%]	Mn [wt.%]	O [wt.%][(a)]
1	7.5	43.5	2.4	40.3	6.3
2	72.0	5.0	1.4	0.6	20.9
3	88.4	5.9	2.3	0.5	2.8
4	80.7	10.5	1.4	0.6	6.8

(a) Oxygen values can only be used as relative differences between measurements, because of uncertainties in the lower energy range of the EDXS spectra.

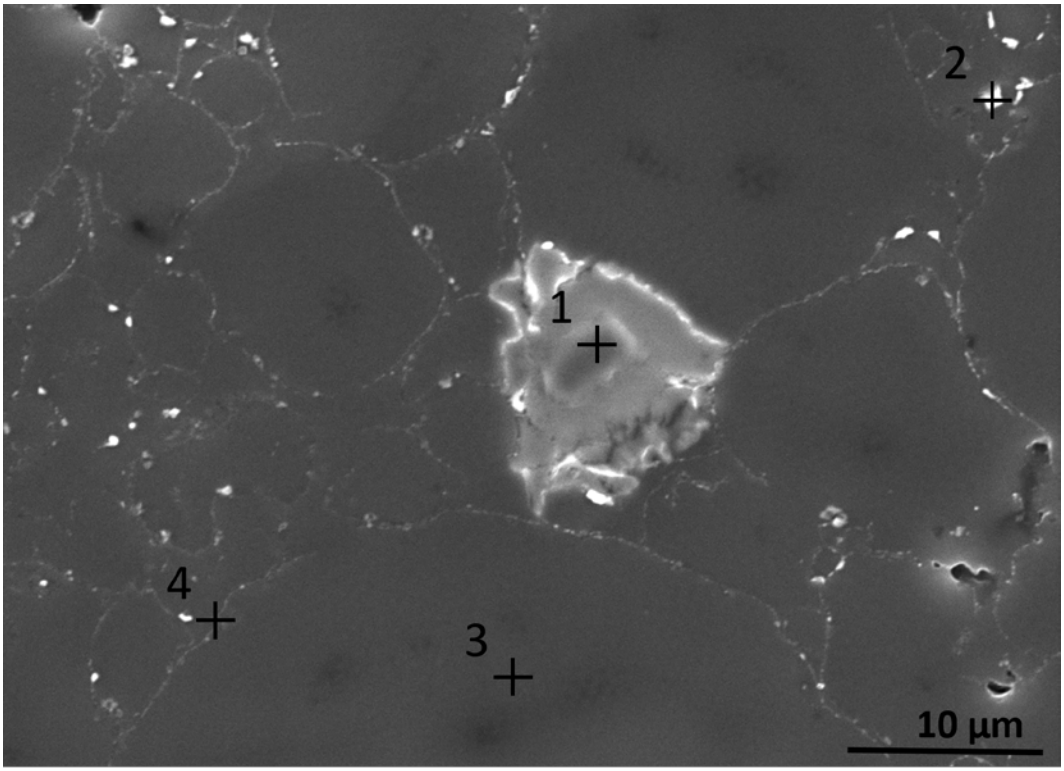

Figure 3. SEM microstructure of AZ81 MIM+T4 in SE mode.

Table 2. Results of EDXS measurements on Figure 3

Point	Mg [wt.%]	Al [wt.%]	Zn [wt.%]	Mn [wt.%]	O [wt.%][(a)]
1	2.5	40.9	2.5	44.9	9.3
2	76.5	7.1	2.6	0.6	13.2
3	83.3	7.2	2.7	1.1	5.7
4	79.3	9.9	2.7	0.6	7.5

The mechanical properties of the processed MIM and MIM+T4 samples as well as literature values for conventionally processed AZ81 are given in **Table 3**. While **Figure 4** displays typical stress strain curves of samples in the as MIM condition (black curve) and in the MIM+T4 condition (red curve). The mechanical properties of the MIM samples show a higher yield strength and a slightly reduced elongation and ultimate tensile strength in comparison to conventional production techniques like permanent mould casting and sand casting (Avedesian

and Baker, 1999). The differences in mechanical properties is presumably caused by the microstructure. The porosity might have a reducing influence on the ultimate tensile strength as well as on the elongation at fracture due to fracture initiating properties of the pores and reduction of the load-bearing cross section (German, 1985). Precipitation of oxides and Al-rich phases might also have a decreasing effect on the ultimate tensile strength and on the elongation at fracture. The higher yield strength compared to as cast material might be due to a strengthening effect of the oxide and Al-rich precipitations on the former particle boundaries. The decrease of the mechanical properties due to the T4 heat treatment is in contrast to the general experience that T4 heat treatment improves the mechanical properties, especially the elongation (Avedesian and Baker, 1999). However, all mechanical properties are reduced by T4 heat treatment. The evaluation of the MIM and MIM+T4 microstructures reveals only minor differences which cannot explain the considerable differences in the mechanical properties.

Table 3. Mechanical properties of AZ81 MIM and MIM+T4 heat treated samples

Condition	Yield Strength (±SD) [MPa]	Ultimate Tensile Strength (±SD) [MPa]	Elongation at Fracture (±SD)
AZ81 MIM	121 (±1)	257 (±5)	7% (±1%)
AZ81 MIM+T4	113 (±2)	226 (±5)	5% (±1%)
AZ81A-T4 sand cast [(a)]	80 - 100	250-290	11% - 14%
AZ81A-T4 permanent mold[(a)]	75 - 95	235-260	7% - 13%

(a) taken from (Avedesian and Baker, 1999)

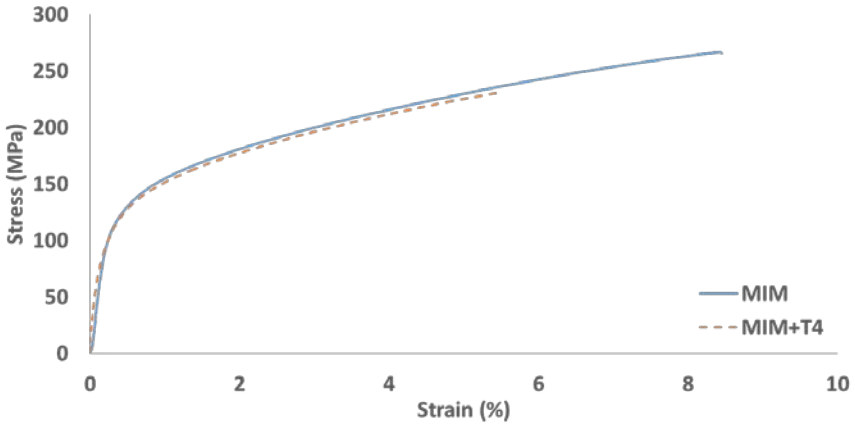

Figure 4. Typical stress strain curve of AZ81 MIM (black) and MIM+T4 (red, dotted) tensile test

For Mg-Ca alloys it is reported that grain growth is stopped at former powder particles during the sintering process due to the existence of oxides at the particle boundaries (Wolff et al. 2014).

The former powder particle boundaries are still visible in **Figure 2(b)** leading to the preliminary assumption that grain size is not affected by T4 heat treatment. However, to explain the reduction of the mechanical properties EBSD measurements were performed to detect a possible grain growth exceeding the oxides at the former particle boundaries. **Figure 5** shows the results of the EBSD measurements. The grains are showing an irregular interlocked camouflage like pattern. **Figure 6(a)** displays a higher magnification of the EBSD MIM measurement, while **Figure 6(b)** shows an EBSD measurement of Mg-0.9Ca MIM for comparison. For Mg-0.9Ca grain growth stops at former particle boundaries. For the AZ81 material grain boundaries still follow the former particle boundaries, but grains are not limited to single powder particles as indicated by the black-rimmed circles. This leads to the conclusion that the oxides at the particle boundaries act as obstacles for the grain growth process, but do not completely block the growth. When the EBSD results of the MIM material (**Figure 5 a**) and the MIM+T4 material (**Figure 5 b**) are compared, it can be seen that the pattern of the MIM+T4 heat treated material is much coarser. Grain size measurements by linear intercept method give a grain size of 45 µm for the MIM material and 62 µm for the MIM+T4 material. These values cannot be used as absolute values for the grain size, because the linear intercept method is not ideal for measuring grains with such an irregular shape. However, this measurement confirms the optical appearance of grain growth. This grain growth is most likely the reason for the decrease of mechanical properties caused by the T4 heat treatment. Future heat treatment at lower temperatures and shorter times or a direct ageing after MIM without T4 may result in less grain growth and improvement in mechanical properties.

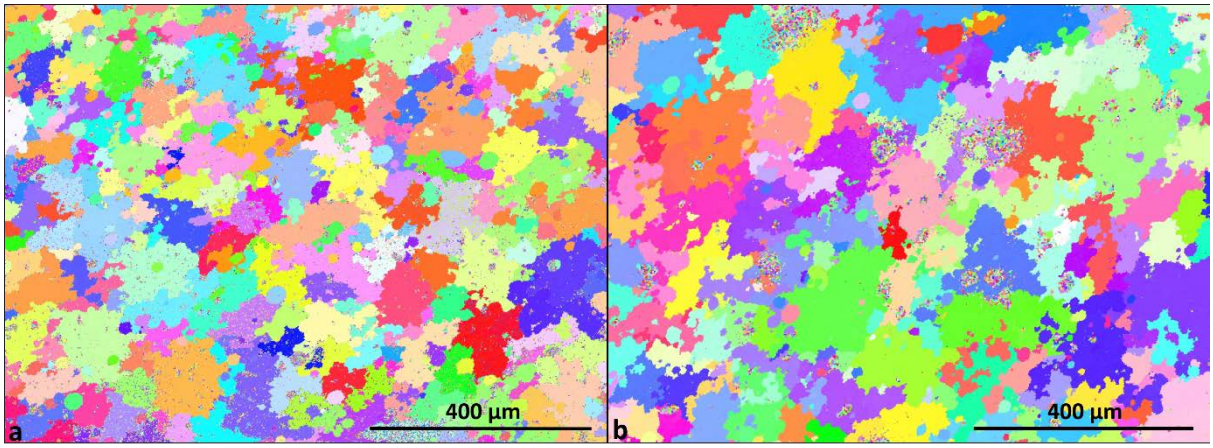

Figure 5. (a) EBSD AZ81 MIM grain size 45 µm, (b) EBSD AZ81 MIM+T4 grain size 62 µm

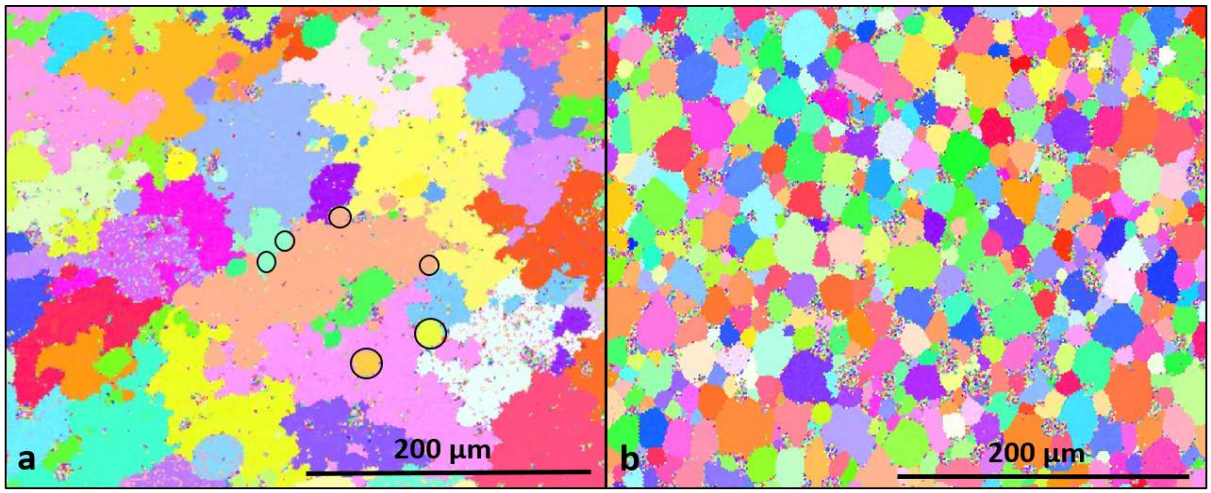

Figure 6. (a) Higher magnification of EBSD AZ81 MIM. The shape of the former powder particles can still be observed as indicated with the black-rimmed circles, (b) EBSD measurement of Mg-0.9Ca

Conclusions

AZ81 could be successfully introduced into the MIM process. The short sintering time and high mechanical properties compared to MIM of Mg-0.9Ca highlights the potential for economic production of small and complex near net shape Mg parts in large quantities by using AZ81 in the MIM process. The mechanical properties of the material in the MIM condition obtain yield strength of approximately 120 MPa, an ultimate tensile strength of approximately 255 MPa and an elongation at fracture of approximately 7%. Ultimate tensile strength as well as the elongation at fracture match those of conventionally produced material like cast in T4 condition. The higher yield strength might be caused due to a strengthening effect of the oxide and Al-rich phase precipitations at the former powder particle boundaries. Applying T4 heat treatment at

420 °C for 10 hours did not improve the mechanical properties of the MIM material; it even decreased them as a result of a grain growth effect that could be proven using EBSD measurements. Following an in-depth literature review this is the first time that grain growth has been observed for Mg-MIM material. Adjusting the temperature and time for the T4 or ageing heat treatment could be an option to improve mechanical properties further compared to the as-MIM material. The short sintering time of approximately 4 hours, in comparison to up to 64 hours for Mg and Mg-Ca alloys, in combination with higher strength indicates AZ81 is an ideal candidate for MIM processing. It is thus possible for AZ81 to be used for economical production technique of complex shaped Mg-parts in high quantities that match the properties of cast + T4 heat treatment without an additional heat treatment step.

Acknowledgements

The authors like to thank Petra Fischer for the help on conducting the EBSD measurements.

This work was funded by Helmholtz Zentrum Geesthacht GmbH and Element 22 GmbH.

Data availability statement

The raw/processed data required to reproduce these findings cannot be shared at this time as the data also forms part of an ongoing study. Please contact the authors for detailed information.

References

Avedesian, M.M., Baker, H., 1999. Magnesium and Magnesium Alloys, ASM International, Materials Park, OH, USA.

Burke, P., Kipouros, G.J., Fancelli, D., Laverdiere, V., 2013. Sintering Fundamentals of Magnesium Powders, Can. Metall. Q., 48, 123-132.

Čapek, J., Vojtěch, D., 2013. Properties of porous magnesium prepared by powder metallurgy, Mater. Sci. Eng. C, 33, 564-569.

Čapek, J., Vojtěch, D., 2014. Effect of sintering conditions on the microstructural and mechanical characteristics of porous magnesium materials prepared by powder metallurgy, Mater. Sci. Eng. C, 35, 21-28.

CompuTherm LLC, 2017. http://www.computherm.com, Pandat^{TM} 2017 with PanMagnesium 2017 database.

German, R.M., 1985. Liquid Phase Sintering, Plenum Press, New York, USA.

German, R.M., 1990. Powder Injection Molding, Metal Powder Industries Federation, Princeton, New Jersey

Ha, W., Kim, Y.-J., 2006. Effects of cover gases on melt protection of Mg alloys, J. Alloys Compd., 422, 208-213.

Harun, M. R., Muhamad, N., Sulong, A. B., Nor, N. H. M., Jamaludin, K. R., Ibrahim, M. H., 2010. Solvent Debinding Process for ZK60 Magnesium Alloy Mim Compact, J. Teknologi, 59, 159-168.

Harun, M.R., Muhamad, N., Sulong, A.B., Nor, N.H. M., Ibrahim, M.H.I., 2010. Rheological Investigation of ZK60 Magnesium Alloy Feedstock for Metal Injection Moulding using Palm Stearin Based Binder System, Appl. Mech. Mater., 44-47, 4126-4130.

Kainer, K.U., 2003. Magnesium Alloys and Technologies, WILEY-VCH, Weinheim, Germany, pp. 1-23.

Mordike, B.L., Ebert, T., 2001. Magnesium: Properties -applications - potential, Mater. Sci. Eng.: A, 302, 37-45.

Nishiyama, K., Matsui, R., Ikeda, Y., Niwa, S., Sakaguchi, T., 2003. Damping properties of a sintered Mg–Cu–Mn alloy, J. Alloys Compd., 355, 22-25.

Obasi, G.C., Ferri, O.M., Ebel, T., Bormann, R., 2010. Influence of processing parameters on mechanical properties of Ti–6Al–4V alloy fabricated by MIM, Mater. Sci. Eng. A, 527, 3929-3935.

Ohno, M., Mirkovic, D., Schmid-Fetzer, R., 2006. Liquidus and solidus temperatures of Mg-rich Mg–Al–Mn–Zn alloys, Acta Mater., 54, 3883-3891.

Schaper, J.G., Wolff, M., Ebel, T., Dahms, M., Willumeit-Römer, R., 2017. MIM Processing of Complex Mg-Alloys, Proceedings of the EuroPM2017, Milan, Italy.

Taleghani, M.A.J., 2014. Processing and properties of high performance 7075 Al and AZ91 Mg powder metallurgy alloys, Doctoral Thesis, Universidad Carlos III de Madrid.

Wen, C.E., Mabuchi, M., Yamada, Y., Shimojima, K., Chino, Y., Asahina, T., 2001. Processing of biocompatible porous Ti and Mg, Scripta Mater., 45, 1147-1153.

Wen, C.E., Yamada, Y., Shimojima, K., Chino, Y., Hosokawa, H., Mabuchi, M., 2004. Compressibility of porous magnesium foam: dependency on porosity and pore size, Mater. Lett., 58, 357-360.

Wiese, B., Mendis, C. L., Tolnai, D., Szakacs, G., Stark, A., Schell, N., Reichel, H.-P., Brueckner, R., Hort, N., Kainer, K. U., 2014. In Situ Synchrotron Radiation Diffraction during Melting and Solidification of Mg-Al Alloys Containing CaO, Magnesium Technology 2014, Proceedings of 143rd Annual Meeting & Exhibition TMS 2014, San Diego, CA, USA.

Witte, F., Hort, N., Vogt, C., Cohen, S., Kainer, K.U., Willumeit, R., Feyerabend, F., 2008. Degradable biomaterials based on magnesium corrosion, Curr. Opin. Solid. St. M., 12, 63-72.

Wolff, M., Ebel, T., Dahms, M., 2010. Sintering of Magnesium, Adv. Eng. Mater., 12, 829-836.

Wolff, M., Schaper, J.G., Dahms, M, Ebel, T., Kainer, K.U., Klassen, T., 2014. Magnesium Powder Injection Moulding for biomedical application, Proceedings of the EuroPM2014, EPMA, Salzburg, Austria.

Wolff, M., Schaper, J.G., Dahms, M., Ebel T., Willumeit-Römer, R., Klassen, T., 2018. Metal Injection Molding (MIM) of Mg-Alloys, Proceedings of 147th Annual Meeting & Exhibition TMS 2018, Phoenix, AZ, USA, 239-251

Wolff, M., Schaper, J.G., Suckert, M.R., Dahms, M., Ebel, T., Willumeit-Römer, R., Klassen, T., 2016a. Enhancement of Thermal Debinding and Sintering of Biodegradable MIM-Magnesium Parts for Biomedical Applications, Proceedings of the World PM2016, Hamburg, Germany.

Wolff, M., Schaper, J.G., Suckert, M.R., Dahms, M., Feyerabend, F., Ebel, T., Willumeit-Römer, R., Klassen, T., 2016b. Metal Injection Molding (MIM) of Magnesium and Its Alloys, Metals, 6, 118.

Wolff, M., Wiese, B., Dahms, M., Ebel, T., 2011. Binder development for Magnesium Powder Injection Moulding, Proceedings of the Euro PM 2011, EPMA, Barcelona, Spain.